Journal of Magnetic Resonance **140,** 131–140 (1999)
Article ID jmre.1999.1827, available online at http://www.idealibrary.com on IDEAL®

Experimental Aspects of Multidimensional Solid-State NMR Correlation Spectroscopy

A. Ramamoorthy,[1] C. H. Wu,[2] and S. J. Opella[3]

Department of Chemistry, University of Pennsylvania, Philadelphia, Pennsylvania 19104

Received November 18, 1998; revised May 27, 1999

The experimental parameters critical for the implementation of multidimensional solid-state NMR experiments that incorporate heteronuclear spin exchange at the magic angle are discussed. This family of experiments is exemplified by the three-dimensional experiment that correlates the ^{1}H chemical shift, ^{1}H–^{15}N dipolar coupling, and ^{15}N chemical shift frequencies. The broadening effects of the homonuclear ^{1}H–^{1}H dipolar couplings are suppressed using flip–flop (phase- and frequency-switched) Lee–Goldburg irradiations in both the ^{1}H chemical shift and the ^{1}H–^{15}N dipolar coupling dimensions. The experiments are illustrated using the ^{1}H and ^{15}N chemical shift and dipolar couplings in a single crystal of ^{15}N-acetylleucine. © 1999 Academic Press

Key Words: **spin exchange at the magic angle; Lee–Goldburg; multiple pulse; PISEMA; HETCOR.**

INTRODUCTION

It is generally more difficult to resolve and characterize resonances from individual molecular sites with solid-state NMR experiments than it is with the corresponding solution NMR experiments. This is because of the severe line broadening that results from the operative nuclear spin-interactions, including chemical shift and homonuclear and heteronuclear dipolar couplings, in the absence of motional averaging. The key to obtaining high-resolution solid-state NMR spectra that reveal the spectral parameters resulting from the spin-interaction of interest without interference from excessive linebroadening from the same or different spin-interactions lies in the concept and practice of selective averaging (*1*). In most implementations of selective averaging, the unwanted spectroscopic effects of the spin-interactions are either suppressed or placed in another frequency dimension. For example, chemical shifts and heteronuclear dipolar coupling frequencies can be readily measured with separated-local-field (SLF) spectroscopy, which was the first and remains the definitive example of the multidimensional approach to selective averaging in solid-state NMR spectroscopy (*2*). Each heteronuclear dipolar coupling frequency resolved on the basis of chemical shift frequency reflects the internuclear distance and orientation of the internuclear vector with respect to the direction of the applied magnetic field for a particular molecular site. Accurate and precise measurements of the dipolar coupling frequencies from the interactions between a dilute spin (e.g., ^{13}C or ^{15}N) and abundant spins (^{1}H) are complicated by the residual effects of the very strong homonuclear ^{1}H–^{1}H dipolar couplings in most organic and biomolecules. Therefore, it is essential to implement an effective method of suppressing the homonuclear ^{1}H–^{1}H dipolar couplings without drastically scaling the heteronuclear dipolar couplings of interest. A variety of multiple pulse sequences, including WAHUHA (*3*), MREV-8 (*4*), and Lee–Goldburg off-resonance irradiation (*5*), have been applied during the t_1 interval of conventional two-dimensional SLF experiments to suppress homonuclear ^{1}H–^{1}H dipolar couplings while the heteronuclear dipolar couplings are effecting the evolution of the dilute spin magnetization generated by cross-polarization. All of these procedures have the undesirable side effect of significantly scaling down the heteronuclear dipolar couplings when applied during a conventional t_1 period. Further, an implicit requirement of the SLF experiment, when performed at high fields, is the need for an additional time period to refocus the chemical shift of the dilute nucleus of interest (*6*), and this can result in a substantial loss in magnetization due to the short T_2 relaxation times in some crystals and most biopolymers. Similar difficulties are encountered in heteronuclear chemical shift correlation experiments (*7–9*). As a result, the initial three-dimensional solid-state NMR experiments (*10, 11*) based on conventional two-dimensional SLF and heteronuclear correlation (HETCOR) experiments had limited applicability to proteins.

In contrast, experiments based on polarization-inversion spin-exchange (*12–18*) take advantage of the spin-lock in the rotating frame to reduce the effects of spin-diffusion among the ^{1}H nuclei with minimal scaling of the heteronuclear dipolar couplings. For example, we have shown that the PISEMA (polarization inversion spin exchange at the magic angle) pulse sequence is highly effective at suppressing the effects of the

[1] Present address: Biophysics Research Division and Department of Chemistry, The University of Michigan, Ann Arbor, MI 48109.

[2] Present address: Quantum Magnetics, 7740 Kenamar Ct., San Diego, CA 92121.

[3] To whom correspondence should be addressed at Department of Chemistry, University of Pennsylvania, 231 South 34th Street, Philadelphia, PA 19104. Fax: (215) 573-2123. E-mail: opella@sas.upenn.edu.

1090-7807/99 $30.00

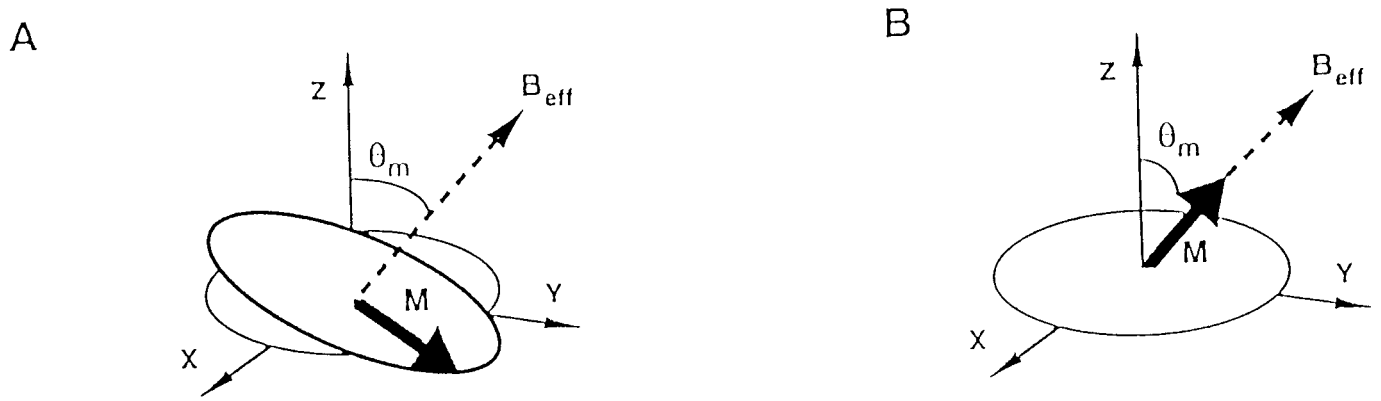

FIG. 1. Vector diagrams that illustrate the effects of Lee–Goldburg irradiation on magnetization. A. Direct application for decoupling. B. Spin-lock at the magic angle.

homonuclear ^{1}H–^{1}H dipolar couplings while scaling the heteronuclear dipolar couplings by only 0.82 (*19*). As a result, the effective resolution in the heteronuclear dipolar frequency dimension of PISEMA spectra is vastly improved compared to that in SLF experiments employing conventional t_1 evolution of the dipolar frequencies, regardless of which homonuclear decoupling sequence is applied to the ^{1}H resonances during that interval. A family of double- and triple- resonance pulse sequences incorporating SEMA (spin exchange at the magic angle) have been developed; they enable the measurement and correlation of multiple frequencies in single-crystal (*20–24*) and oriented samples (*25–33*) and the characterization of the chemical shift and dipolar coupling interaction tensors in spinning (*34, 35*) and stationary (*36–38*) powder samples. In applications to oriented samples of ^{15}N-labeled peptides and proteins, the ^{1}H chemical shift, ^{1}H–^{15}N heteronuclear dipolar coupling, and ^{15}N chemical shift frequencies provide resolution among backbone amide sites, as well as the spectral parameters used to determine the orientations of peptide planes with respect to the direction of the applied magnetic field (*27, 28, 31*). It is possible to obtain completed resolved spectra of uniformly ^{15}N-labeled proteins with this approach that provide sufficient orientational constraints information to determine the three-dimensional structures of proteins (*28*). Triple resonance versions of these experiments are applicable to applicable to ^{13}C- and ^{15}N-labeled proteins (*23, 24, 29*) and give opportunities for making sequential resonance assignments and measuring additional structural parameters for backbone and side chain sites.

Off-resonance continuous ^{1}H irradiation is remarkably effective at suppressing homonuclear ^{1}H–^{1}H dipolar couplings (*5*). It was cast in terms of the coherent averaging theory of multiple pulse experiments by Mehring and Waugh (*39*), and further developed by Griffin and co-workers (*40, 41*). Lee–Goldburg experiments involve the application of RF irradiation, B_1, at an off-resonance frequency, B_{off}, to establish an effective field at the magic angle, θ_m, 54.7° with respect to the external magnetic field, B_o. The efficiency of the procedure is improved by the implementation of the (phase- and frequency-switched) flip–flop Lee–Goldburg pulse sequence where the direction of the effective field is alternated every 2π rotation

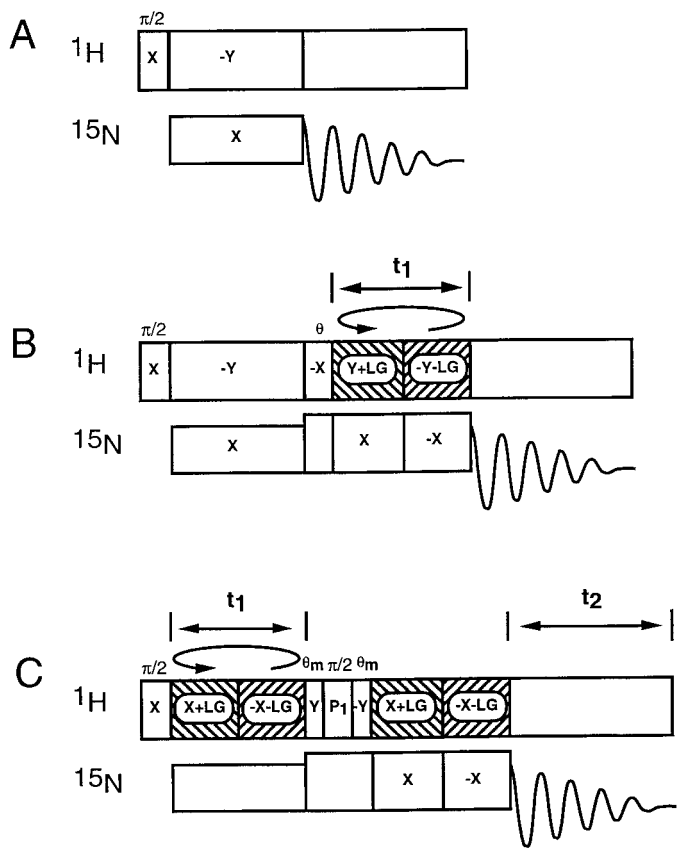

FIG. 2. Pulse sequence diagrams. A. One-dimensional cross-polarization. B. Two-dimensional PISEMA. C. Two-dimensional HETCOR. X, $-X$, Y, $-Y$ specify quadrature phases. +LG, −LG specify positive and negative frequencies that fulfill the Lee–Goldburg condition. $\pi/2$ corresponds to a 90° pulse, θ corresponds to 35.3° pulse, and θ_m corresponds to a 54.7° pulse. Quadrature detection can be accomplished with appropriate phase cycling of the pulse $P1$ and the receiver (*45*).

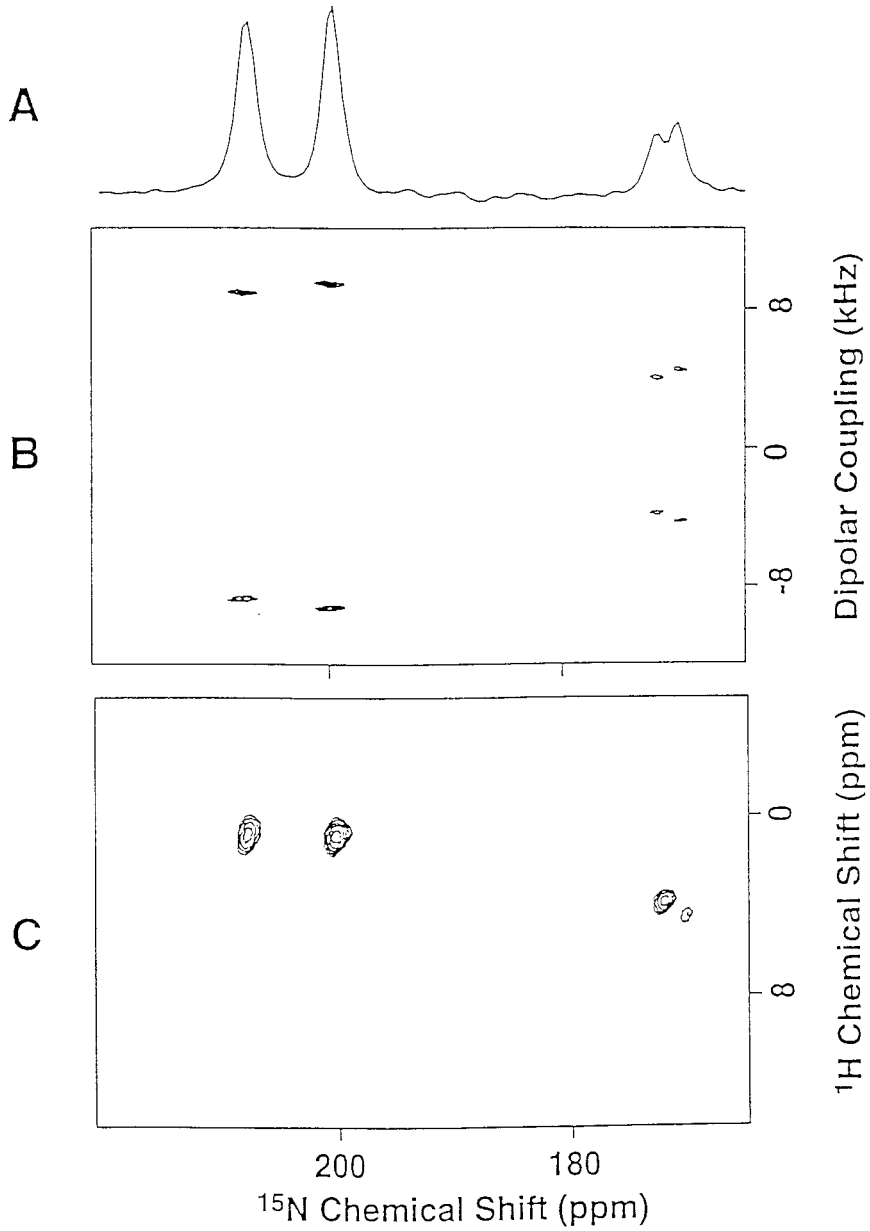

FIG. 3. NMR spectra of a single crystal of ^{15}N-acetylleucine. A. One-dimensional ^{15}N chemical shift spectrum. B. Two-dimensional ^{1}H/^{15}N PISEMA spectrum. C. Two-dimensional ^{1}H/^{15}N HECTOR spectrum.

(*41*). This is straightforward to implement with modern frequency synthesizers, although Mehring and Waugh previously used an external dc field to create the appropriate offset (*38*). Since flip–flop Lee–Goldburg is a windowless sequence, measurement of its line-narrowing efficiency by observing the signal stroboscopically after each cycle is not possible with simple one-dimensional experiments. However, this can be readily accomplished in two-dimensional experiments. When implemented directly, both Lee–Goldburg and flip–flop Lee–Goldburg sequences suppress the ^{1}H–^{1}H dipolar couplings and scale the frequencies associated with other interactions, including ^{1}H chemical shift and heteronuclear dipolar couplings by the factor $\cos(54.7°) = 0.58$. The relatively large scaling factor is a limitation of Lee–Goldburg sequences when applied during the evolution period for ^{1}H chemical shift or heteronuclear dipolar couplings in the pulse sequences for conventional multidimensional experiments. Notably, the scale factor is a much more favorable 0.82 when the Lee–Goldburg irradiation is applied as part of SEMA sequences (*19*). The scaling and line narrowing of Lee–Goldburg irradiation have been analyzed for a variety of experimental conditions (*42*).

Thus, the flip–flop Lee–Goldburg procedure can be incorporated into multidimensional solid-state NMR experiments in two distinct ways. In the two-dimensional HETCOR experi-

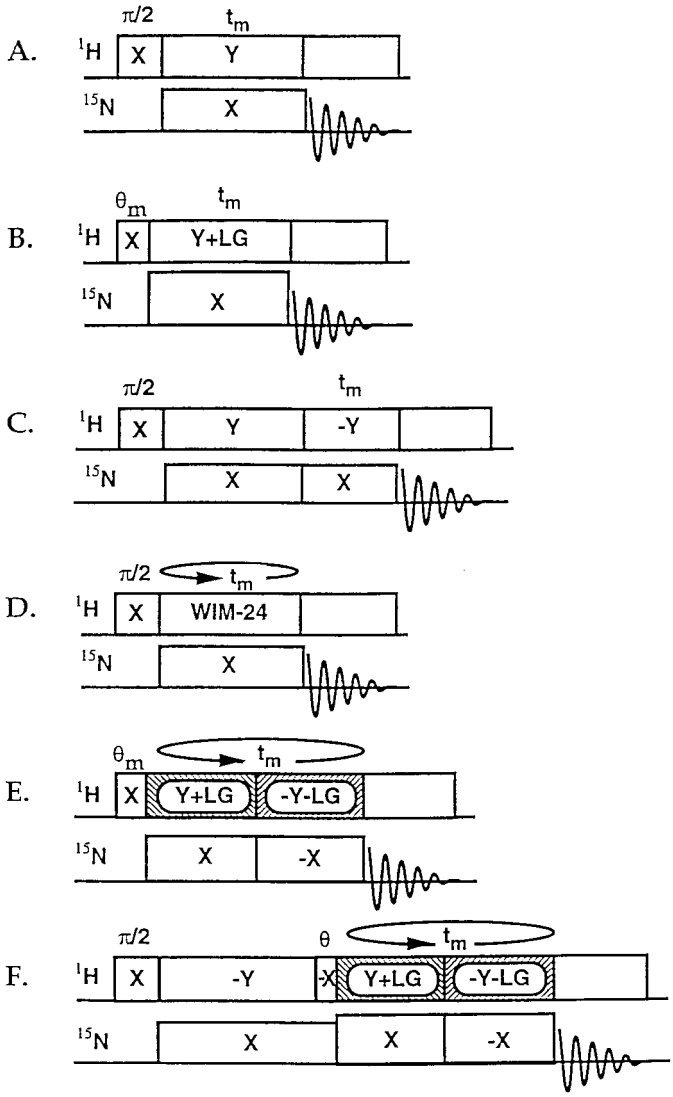

FIG. 4. Pulse sequence diagrams for the experimental procedures used to effect transfer of magnetization between ^{1}H and ^{15}N nuclei. The letters correspond to the plots in Fig. 5. A. Conventional cross-polarization (CP). B. CP with Lee–Goldburg irradiation. C. Polarization-inversion of the ^{1}H magnetization following the CP sequence. D. CP with WIM-24 irradiation. E. CP with SEMA. F. PISEMA.

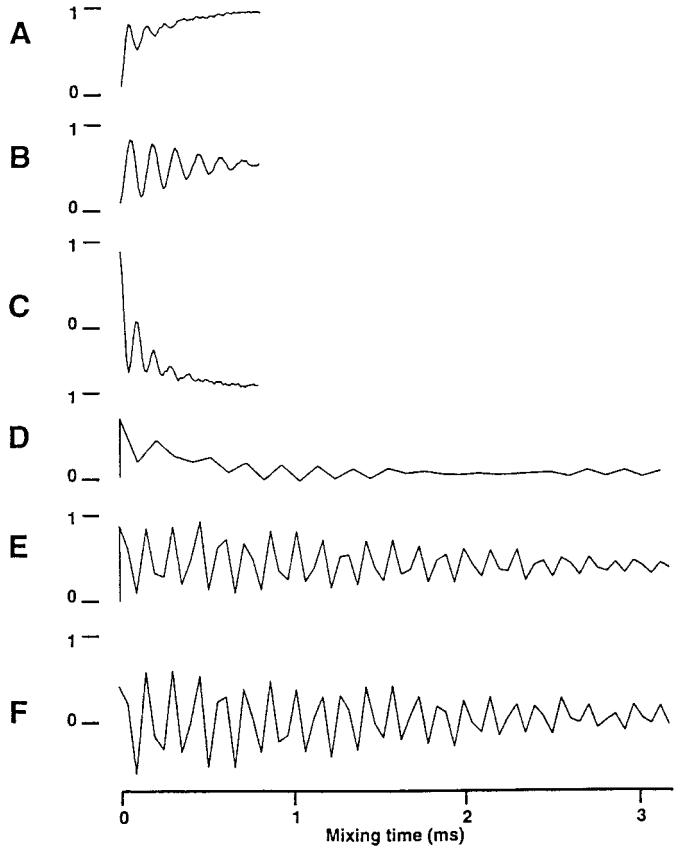

FIG. 5. Plots of the amplitude corresponding to magnetization as a function of the length of the transfer interval. The letters correspond to the pulse sequences in Fig. 4.

$$\Omega = (\gamma_I\gamma_S h/r_{IS}^3)[3\cos^2(\theta) - 1]\sin(\epsilon_I)\sin(\epsilon_S) \quad [1]$$

$$= \kappa\gamma_I\gamma_S h/r_{IS}^3[3\cos^2(\theta) - 1], \quad [2]$$

where $\kappa = \sin(\epsilon_I) \times \sin(\epsilon_S)$ is the scaling factor for the magic angle spin locking sequences; ϵ_I and ϵ_S define the directions of the effective spin locking fields for the I (^{1}H) and S (^{15}N or ^{15}C) nuclei, with respect to the external magnetic field. In both

ment, it is implemented during t_1 in order to suppress homonuclear dipolar couplings while measuring the ^{1}H chemical shift frequencies (*20*, *43*); here the magnetization evolves in a tilted frame, as shown in Fig. 1A. In SEMA sequences (*19*), it is used to lock the ^{1}H magnetization along the magic angle, as shown in Fig. 1B. The SEMA sequences are highly effective because ^{1}H–^{1}H dipolar couplings are suppressed and the ^{1}H chemical shift does not evolve during the spin-lock interval. The oscillating frequency, Ω, and the frequency of the heteronuclear dipolar coupling between two nuclei ($S = \frac{1}{2}$ and $I = \frac{1}{2}$) are related by

TABLE 1

Experimental Parameters for an Arbitrary Orientation of the NAL Single Crystal Measured from the Three-Dimensional NMR Spectrum

Molecule	δ_{15N} (ppm)[a]	D_{NH} (kHz)	δ_{1H} (ppm)[b]
a	171.0	8.42	4.8
b	172.5	7.42	4.0
c	200.5	18.58	1.1
d	208.0	17.58	1.0

[a] Relative to $(^{15}NH_4)_2SO_4$.
[b] Relative to TMS.

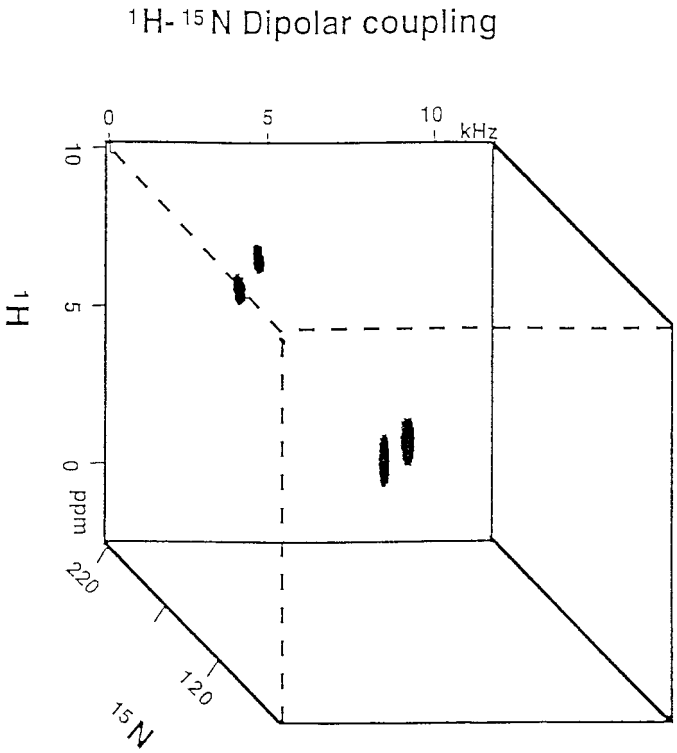

FIG. 6. Three-dimensional ^{1}H chemical shift/^{15}N/^{1}H–^{15}N heteronuclear dipolar coupling/^{15}N chemical shift correlation spectrum of a single crystal of ^{15}N-acetylleucine.

PISEMA and SEMA experiments, $\epsilon_I = 54.7°$ and $\epsilon_S = 90°$ and, therefore, κ is 0.82. θ defines the direction of the I–S bond with respect to the magnetic field; r_{IS} is the separation between the I nucleus and the S nucleus (the bond length).

RESULTS AND DISCUSSION

One- and two-dimensional experimental NMR spectra obtained from a single-crystal sample of ^{15}N-acetylleucine (NAL) using the pulse sequences diagrammed in Fig. 2 are shown in Fig. 3. The one-dimensional ^{15}N chemical shift spectrum obtained with the conventional cross-polarization pulse sequence shown in Fig. 3A has four ^{15}N resonances, two of which partially overlap. The linewidths of these resonances are about 4 ppm when adequate ^{1}H decoupling is applied during data acquisition. The resonances are resolved because the unique orientations of the amide groups in the four molecules of the unit cell of the single crystal result in different ^{15}N chemical shift frequencies. The two-dimensional ^{1}H–^{15}N heteronuclear dipolar coupling/^{15}N chemical shift spectrum obtained using the PISEMA pulse sequence is shown in Fig. 3B. The linewidths in the dipolar dimension are approximately 200 Hz, which reflects the highly effective decoupling of ^{1}H–^{1}H homonuclear interactions by the flip–flop Lee–Goldburg irradiation in this procedure. One of the major disadvantages of conventional SLF experiments can be loss of magnetization due to T_2 relaxation during t_1, especially if a ^{15}N chemical shift refocusing interval is utilized. In contrast, in PISEMA experiments, the magnetization is always locked in the rotating frame where its slower decay reflects the generally longer $T_1\rho$ relaxation times.

The indirectly detected free induction decays from the heteronuclear dipolar coupling oscillations shown in Fig. 5 were obtained by applying the heteronuclear spin exchange pulse sequences shown in Fig. 4. This comparison demonstrates how the various schemes for homonuclear ^{1}H–^{1}H decoupling affect the heteronuclear ^{1}H–^{15}N dipolar interaction. In Figs. 5B and 5D, Lee–Goldburg and a windowless version of an isotropic multiple pulse sequence (WIM-24) (*8, 43*), respectively, are used for homonuclear ^{1}H–^{1}H decoupling and to lock the ^{1}H magnetization along the effective field direction. The RF field strength in the ^{15}N channel is matched to the effective field of the ^{1}H channel during the mixing period. These procedures are adequate for determining the dipolar oscillations associated with the ^{15}N resonance labeled **a** (Table 1), which correspond to a heteronuclear dipolar coupling of 17.58 kHz. The goal is to implement a pulse sequence, which minimizes the scaling of the ^{1}H–^{15}N dipolar coupling frequencies with maximum suppression of the homonuclear ^{1}H–^{1}H dipolar couplings. This would enable the observation of oscillation of the ^{15}N magnetization with a frequency corresponding to the scaled ^{1}H–^{15}N dipolar coupling as a function of the mixing time. However, it is well known that the buildup of magnetization during conventional on-resonance spin-lock cross-polarization reaches a steady state due to the effects of ^{1}H–^{1}H spin diffusion in most chemical and biochemical samples, after the initial strong dipolar oscillations. Results using Lee–Goldburg off-resonance irradiation are generally better than those obtained with polarization-inversion cross-polarization and WIM-24, although the results of WIM-24 for smaller dipolar couplings, for example, the ^{15}N resonances labeled **a** and **b**, are better than those with larger dipolar couplings, such as those labeled **c** and **d**. In pulse sequences with longer cycle times, the oscillations due to larger dipolar couplings cannot be sampled correctly because they are aliased. Thus, there are advantages to using homonuclear decoupling pulse sequences with short cycle times. This becomes even more important when larger ^{1}H–^{13}C dipolar couplings are examined (*24*).

The data show that the SEMA and PISEMA pulse sequences, which have the same favorable scaling factor, result in significant extensions of the dipolar free induction decays. The dipolar oscillations typically last 4 ms after the ^{15}N magnetization is spin-locked. In practice, a 10-ms spin lock of the ^{15}N magnetization with phase-alternated RF irradiation results in the loss of only 5% of the initial magnetization. This compares to a loss of roughly 10% of the magnetization with continuous irradiation under the same conditions. Continuous and flip–flop ^{1}H Lee–Goldburg irradiation result in loses of 15 and 20%, respectively, over 10 ms. This suggests that the loss of magnetization and damping of the dipolar oscillations ob-

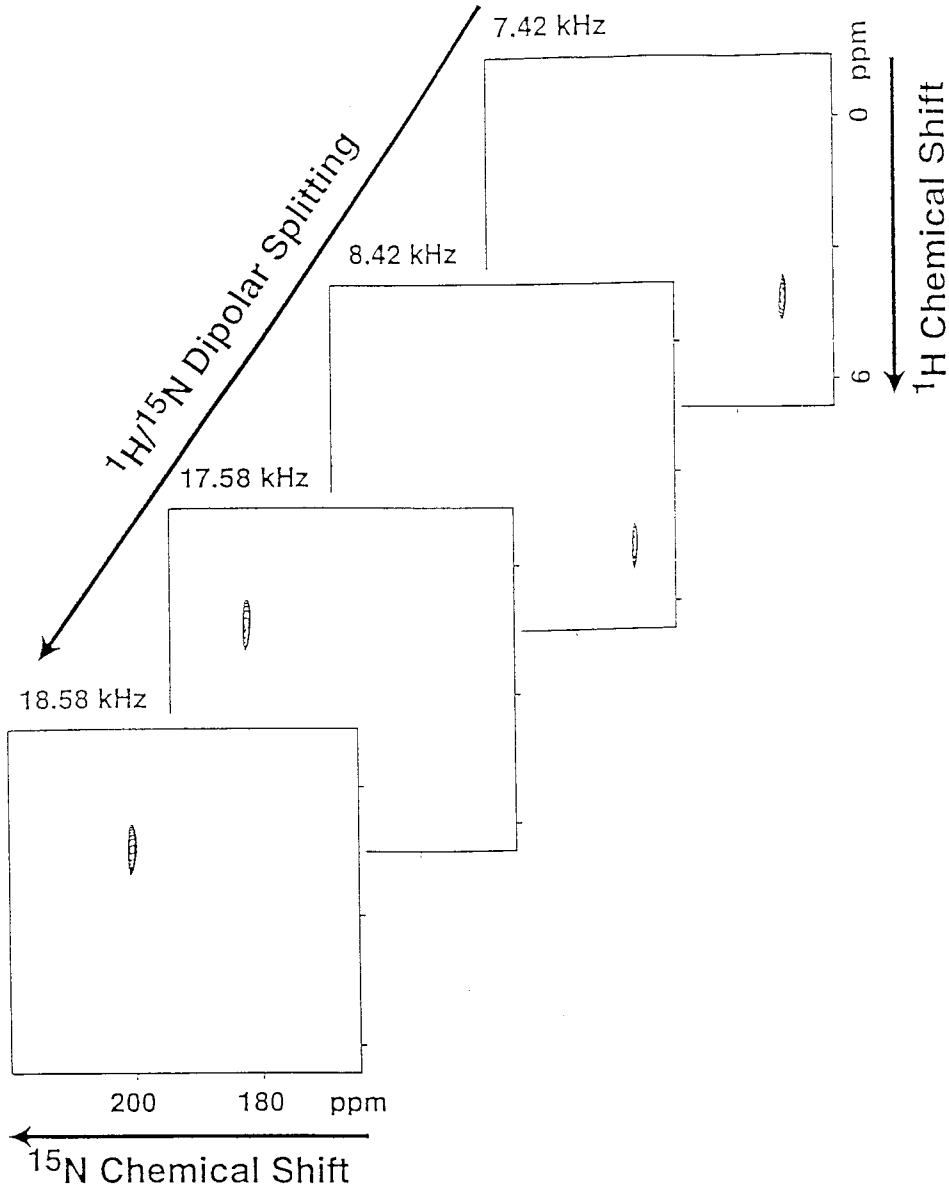

FIG. 7. Two-dimensional HETCOR planes extracted from the three-dimensional data set shown in Fig. 6. Each plane is associated with the ^1H–^{15}N heteronuclear dipolar coupling frequency from one molecule of *N*-acetylleucine.

served with mixing times longer than 4 ms in PISEMA experiments are not due to inefficiencies of the individual spin-lock procedures. While there may be some loss of magnetization due to imperfect synchronization of the phase and frequency shifts in the ^1H RF irradiation and the phase shifts in the ^{15}N RF irradiation, the loss of magnetization during t_1 could also reflect effects of the couplings of the ^{15}N and its attached ^1H with more distant hydrogens. In NAL there are several hydrogens, in addition to the directly bonded one, within 3 Å of the amide ^{15}N, that could contribute to the damping of the dipolar oscillations. Alternatively, the damping could result from the unaveraged higher order terms of the homonuclear ^1H–^1H dipolar Hamiltonian with flip–flop Lee–Goldburg irradiation.

Correlation of ^1H and ^{15}N chemical shift frequencies is demonstrated in the two-dimensional spectrum in Fig. 3C. ^1H linewidths on the order of 0.8 ppm are associated with the ^{15}N resonances that have 1–3 ppm linewidths in this single-crystal sample. Notably, the ^1H chemical shift frequency associated with each ^{15}N chemical shift frequency is different. Also notable, at some orientations of the crystal, poorly resolved ^{15}N lines can be differentiated by their ^1H chemical shifts. The SEMA mixing sequence leads to in-phase magnetization transfers from the ^1H directly bonded to the ^{15}N that are selective and without phase anomalies regardless of the length of the t_1 interval. Flip–flop Lee–Goldburg irradiation is preferable to BR-24 during the t_1 interval of HETCOR experiments because

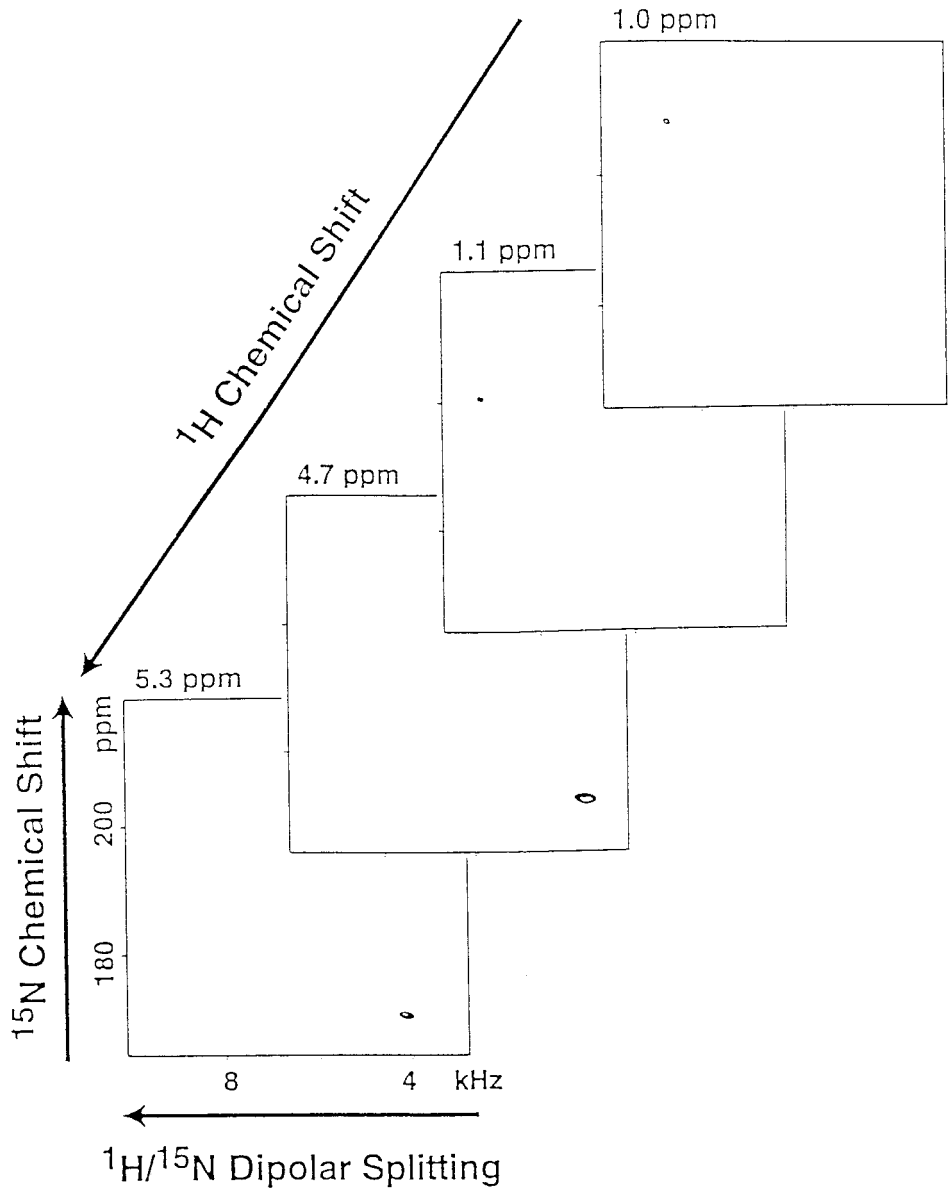

FIG. 8. Two-dimensional PISEMA planes extracted from the three-dimensional data set shown in Fig. 6. Each plane is associated with the ^{1}H chemical shift frequency from one molecule of *N*-acetylleucine.

of its more favorable scaling factor and shorter cycle time. The cycle times of the multiple pulse sequences are crucial when a large spectral width of protons has to be covered with $\pi/2$ pulse widths >3 μs, which is typically the case for biological samples in relatively large samples in high field magnets.

A three-dimensional correlation spectrum of a single-crystal sample of NAL is shown in Fig. 6. The three-dimensional pulse sequence is similar to that used for the two-dimensional HETCOR sequence shown in Fig. 2C except that the SEMA mixing interval is incremented to generate the heteronuclear dipolar coupling frequency dimension. Two-dimensional planes extracted from the three-dimensional data set are shown in Figs. 7 and 8. Figure 7 contains two-dimensional ^{1}H chemical shift/^{15}N chemical shift spectra for the four different ^{1}H–^{15}N dipolar coupling frequencies and Fig. 8 contains two-dimensional ^{15}N chemical shift/^{1}H–^{15}N dipolar coupling spectra for the four different ^{1}H chemical shift frequencies.

The three-dimensional spectrum in Fig. 6 illustrates the high degree of selectively that can be obtained by implementing effective homo- and heteronuclear decoupling procedures during multiple incremented intervals. In most applications, but especially to uniformly isotopically labeled proteins, it is crucial that the optimal phase- and frequency-switched irradiations be selected and optimized. Many of the parameters tested and optimized for this class of solid-state NMR experiments are illustrated in this Article. Carefully set-up flip–flop Lee–

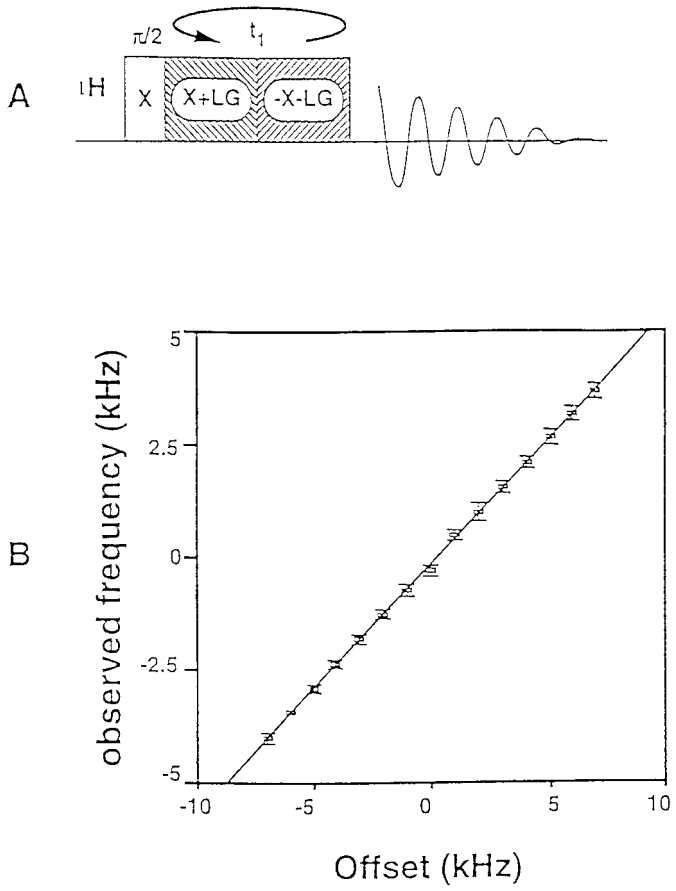

FIG. 9. A. Pulse sequence diagram for the experimental procedure used to measure the scaling factor for the flip–flop Lee–Goldburg irradiation. B. Plot of the observed (scaled) frequency as a function of the actual offset for a sample of liquid water.

Goldburg irradiation is a remarkably flexible tool for performing selective averaging in multidimensional solid-state NMR experiments.

EXPERIMENTAL

The experiments were performed on a homebuilt NMR spectrometer with a 12.9-T wide-bore Magnex 550/89 magnet. The probe had a single 5-mm-ID solenoidal coil double-tuned to the 550- and 55.7-MHz resonance frequencies of the ^{1}H and ^{15}N nuclei.

The sample was a 28-mg single crystal of ^{15}N-acetylleucine, which was prepared by acetylation of 99% enriched ^{15}N-L-leucine (Isotec, Miamisburg, OH) with acetylanhydride in saturated NaOH solution followed by crystallization from aqueous solution. The crystal was placed at an arbitrary orientation in the coil and the measurements were made at ambient temperature. The structure of this crystal form of NAL was determined by X-ray diffraction and found to have four unique molecules in the unit cell.

Radiofrequency irradiations with field strengths corresponding to 61 kHz were applied at both the ^{1}H and the ^{15}N resonance frequencies. The frequency jumps were $\pm$47 kHz to satisfy the Lee–Goldburg off-resonance condition for homonuclear decoupling. During the spin-lock period of PISEMA and SEMA pulse sequences the ^{15}N RF field strength was increased to 77 kHz to match the effective field strength of the ^{1}H RF field strength under these conditions. The chemical shifts of the resonances were referenced to ^{1}H of water at 4.8 ppm and ^{15}N of $(NH_4)_2SO_4$ at 0 ppm, respectively. The slow field drift of the magnet was compensated by supplying a continuous ramp of dc current to the Zo coil of the room temperature shims.

Several tune-up pulse sequences are employed to optimize the relative phases and amplitudes of the RF irradiation using the ^{1}H resonance of a sample of liquid water and the ^{15}N resonances of the NAL crystal sample. The synchronization of the phase and frequency jumps was checked very carefully. Power reflections from the probe, as observed on an oscilloscope with an in-line directional coupler, were minimized under high-power irradiations by careful adjustment of the probe tuning for both on- and off-resonance frequencies. The ^{1}H RF power amplifier was tuned so that the amplitude of its output was the same on- and off-resonance. Differences in the ^{1}H RF power output as a function of frequency offset results in a shift of the observed ^{1}H resonance frequencies in the resulting two-dimensional HETCOR spectrum. The differences in the net flip angles during the first and second halves of each Lee–Goldburg cycle lead to the rotation of the ^{1}H transverse magnetization by a certain angle after each cycle, as if an extra

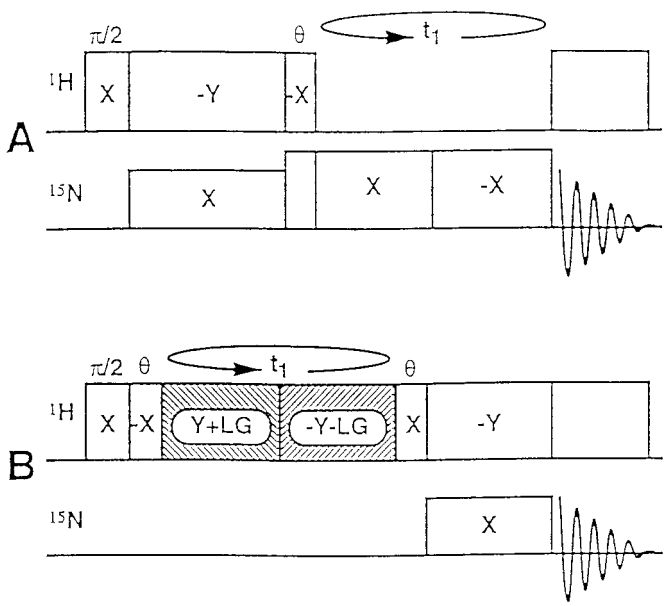

FIG. 10. Pulse sequences diagrams for the experimental procedures used to check the performance of the spectrometer. A. Phase-alternated ^{15}N spin-lock. B. Phase-alternated and frequency-shifted Lee–Goldburg ^{1}H spin-lock.

z-field was applied, resulting in a uniform shift of the entire ^{1}H spectrum. This can be monitored by observing the ^{1}H resonance of water after it evolves under flip–flop Lee–Goldburg irradiation applied during an incremented period in a two-dimensional experiment, as shown in Fig. 9. This stage of the tune-up procedure is very important in order to measure ^{1}H chemical shifts accurately. In addition, an amplitude mismatch during the Lee–Goldburg cycle results in line broadening in both HETCOR and PISEMA spectra due to inefficient homonuclear ^{1}H–^{1}H decoupling and it changes the matching condition, which effects the evolution of the heteronuclear dipolar coupling frequencies.

The pulse sequence diagrammed in Fig. 9A also enables the ^{1}H resonance of water to be used to measure the experimental scaling factor of the flip–flop Lee–Goldburg pulse sequence. Typically, we find the scaling factor to be 0.55 (with an uncertainty of ± 0.01), compared to the theoretical value of 0.58 (Fig. 9B) Two-dimensional HETCOR experiments on a single crystal of NAL are used to optimize the multiple Lee–Goldburg parameters. ^{1}H linewidths are monitored as the jump frequencies and the cycle times of the sequence are varied interactively. The linewidths of the ^{1}H resonances decrease dramatically as the optimal Lee–Goldburg conditions are approached. A control experiment is always performed without the flip–flop Lee–Goldburg spin-lock irradiation in the ^{1}H channel of the PISEMA sequence to check the efficiency of the ^{15}N spin-lock and to confirm that the ^{15}N magnetization does not oscillate as a function of the spin-lock period (Fig. 10A). Similarly, the ^{1}H magnetization following the initial 90° preparation pulse is spin-locked by the flip–flop Lee–Goldburg irradiation and then transferred via cross-polarization to ^{15}N (Fig. 10B) to test the efficiency of the ^{1}H spin-lock in the PISEMA experiment. These control experiments are important because phase transients due to the phase alternation of high-power pulses during the spin-lock result in imperfect spin-locking. Similar errors can also come from imperfections of the RF phase shifts. These false oscillations look like extra dipolar coupling frequencies in the final spectra; thus the sources must be eliminated during the tune-up procedures. To some extent these frequencies are unavoidable in PISEMA spectra of powder samples; however, they can almost always be eliminated from spectra of single crystal and oriented biopolymer samples. To reduce this problem in powder samples, the PISEMA pulse sequence is modified to have 3π–2π irradiation, as one cycle, instead of 2π–2π (*34*). The extra π pulse refocuses the dephasing magnetization due to the phase transients, while it retains all the benefits of the unmodified PISEMA and is highly effective at minimizing false oscillations. PISEMA and HETCOR experiments were performed with RF field strengths varying from 50 to 75 kHz. The results indicate that the efficiency of these pulse sequences does not deteriorate dramatically when relatively low RF powers are utilized.

ACKNOWLEDGMENTS

We thank K. Valentine for advice. This research was supported by Grant RO1GM29754 from the National Institute of General Medical Sciences Institute, National Institutes of Health, and utilized the Resource for Solid-State NMR of Proteins at the University of Pennsylvania, an NIH-Supported Research Center, supported by Grant P41RR0973 from the Biomedical Research Technology Program, National Center for Research Resources, National Institutes of Health.

REFERENCES

1. U. Haeberlen, "High Resolution NMR in Solids: Selective Averaging," Academic Press, New York (1996).
2. J. S. Waugh, Uncoupling of local field spectra in nuclear magnetic resonance: Determination of atomic positions in solids, *Proc. Natl. Acad. Sci. USA* **73,** 1394–1397 (1976).
3. J. S. Waugh, L. M. Huber, and U. Haeberlen, Approach to high-resolution NMR in solids, *Phys. Rev. Lett.* **20,** 180 (1968).
4. W. K. Rhim, D. D. Elleman, and R. W. Vaughan, Enhanced resolution for solid state NMR, *J. Chem. Phys.* **58,** 1772 (1973).
5. M. Lee and W. I. Goldburg, NMR line-narrowing by a rotating rf field, *Phys. Rev. A* **140,** 1261 (1965).
6. M. G. Munowitz, R. G. Griffin, G. Bodenhausen, and T. H. Huang, Two-dimensional rotational spin-echo nuclear magnetic resonance in solids: Correlation of chemical shift and dipolar interactions, *J. Am. Chem. Soc.* **103,** 2529 (1981).
7. P. Caravatti, G. Bodenhausen, and R. R. Ernst, Heteronuclear solid-state correlation spectroscopy, *Chem. Phys. Lett.* **89,** 363–367 (1982).
8. P. Caravatti, L. Braunshweiler, and R. R. Ernst, Heteronuclear correlation spectroscopy in rotating solids, *Chem. Phys. Lett.* **100,** 305 (1983).
9. J. E. Roberts, S. Vega, and R. G. Griffin, Two-dimensional heteronuclear chemical shift correlation spectroscopy in rotating solids, *J. Am. Chem. Soc.* **106,** 2506 (1989).
10. B. S. Arun Kumar and S. J. Opella, Three-dimensional ^{1}H/^{15}N heteronuclear correlation-^{15}N/^{15}N dilute spin-exchange solid-state NMR spectroscopy, *J. Magn. Reson.* **95,** 417–420 (1991).
11. B. S. Arun Kumar and S. J. Opella, Three-dimensional separated–local-field/dilute-spin-exchange solid-state NMR spectroscopy, *J. Magn. Reson. Ser. A* **101,** 333–336 (1993).
12. M. T. Melchier, "21st Experimnetal NMR Conference," 1981. [Poster and Abstract]
13. N. Zumbulyadis, ^{1}H/^{29}Si cross-polarization dynamics in amorphous hydrogenated silicon, *J. Chem. Phys.* **86,** 1162 (1987).
14. D. G. Cory and W. M. Ritchey, Inversion recovery cross-polarization NMR in solid semicrystalline polymers, *Marcomolecules* **22,** 1611–1615 (1989).
15. P. Tekely and J. J. Delpuech, Mobility and hydrogen distribution in coal as revealed by polarization inverstion in high resolution solid-state C-13 CP/MAS NMR, *Fuel* **68,** 947–949 (1989).
16. P. Tekely, F. Montigny, D. Canet, and J. J. Delpuech, High-resolution dipolar NMR-spectra in rotating solids from depolarization of the rare spin magnetization, *Chem. Phys. Lett.* **175,** 401–406 (1990).
17. P. Palmas, P. Tekely, and D. Canet, Local-field measurements on powder samples from polarization inversion of the rare-spin magnetization, *J. Magn. Reson. A* **104,** 26–36 (1993).
18. W. Xiaoling, Z. Shanmin, and W. Xuewen, Selective polarization

inversion in solid state high-resolution CP MAS NMR, *J. Magn. Reson.* **77,** 343 (1988).

19. C. H. Wu, A. Ramamoorthy, and S. J. Opella, High resolution heteronuclear dipolar solid-state NMR spectroscopy, *J. Magn. Reson.* **109,** 270–272 (1994).

20. A. Ramamoorthy, C. H. Wu, and S. J. Opella, Three-dimensional solid-state NMR experiment that correlates the chemical shift and dipolar coupling frequencies of two heteronuclei, *J. Magn. Reson. B* **107,** 88–90 (1995).

21. A. Ramamoorthy, L. M. Gierasch, and S. J. Opella, Four-dimensional solid-state NMR experiment that correlates the chemical shift and dipolar coupling frequencies of two heteronuclei with the exchange of dilute spin magnetization, *J. Magn. Reson. B* **109,** 112–116 (1995).

22. A. Ramamoorthy, L. M. Gierasch, and S. J. Opella, Three-dimensional solid-state NMR correlation experiment with ^{1}H homonuclear spin exchange, *J. Magn. Reson.* **111,** 81–84 (1996).

23. Z. T. Gu, and S. J. Opella, Three-dimensional ^{13}C shift/^{1}H–^{15}N Coupling/^{15}N shift solid-state NMR correlation spectroscopy, *J. Magn. Reson.* **138,** 193–198 (1999).

24. Z. T. Gu and S. J. Opella, Two- and three-dimensional ^{1}H/^{13}C PISEMA experiments and their application to backbone and sidechain sites of amino acids and peptides, *J. Magn. Reson.,* in press (1999).

25. A. Ramamoorthy, F. M. Marassi, M. Zasloff, and S. J. Opella, Three-dimensional solid-state NMR spectroscopy of a peptide oriented in membrane bilayers, *J. Biomol. NMR* **6,** 329–334 (1995).

26. A. Ramamoorthy, F. M. Marassi, and S. J. Opella, Applications of multidimensional solid-state NMR spectroscopy to membrane proteins, *in* "Dynamics and the Problem of Recognition in Biological Macromolecules" (O. Jardetzky and J. Lefevre, Eds.), p. 237, Plenum Press (1996).

27. R. Jelinek, A. Ramamoorthy, and S. J. Opella, High resolution three-dimensional solid-state NMR spectra of a uniformly ^{15}N-labeled protein, *J. Am. Chem. Soc.* **117,** 12348–1234 (1995).

28. F. M. Marassi, A. Ramamoorthy, and S. J. Opella, Complete resolution of the solid-state NMR spectrum of a uniformly ^{15}N-labeled membrane protein in phospholipid bilayers, *Proc. Natl. Acad. Sci. USA* **94,** 8551–8556 (1997).

29. W. M. Tan, Z. T. Gu, A. C. Zeri, and S. J. Opella, Solid-state NMR triple-resonance backbone assignments in a protein, submitted for publication (1998).

30. Y. Kim, K. Valentine, S. J. Opella, S. L. Schendel, and W. A. Cramer, Solid-state NMR studies of the membrane-bound closed state of the colicin e1 channel domain in lipid bilayers, *Protein Sci.* **7,** 342–348 (1998).

31. S. J. Opella, F. M. Marassi, J. J. Gesell, A. P. Valente, Y. Kim, M. Oblatt-Montal, and M. Montal, Three-dimensional structure of the membrane-embedded M2 channel-lining segment from nicotinic acetylcholine receptors and NMDA receptors by NMR spectroscopy, *Nature Struct. Biol.* **6,** 374–379 (1999).

32. W. M. Tau, R. Jelinek, S. J. Opella, P. Malik, T. D. Terry, and R. N. Perham, Effects of temperature and YZIM mutation on conformational heterogeneity of the major coat protein (p VIII) of filamentous bacteriophage fd, *J. Mol. Biol.* **286,** 787–796 (1999).

33. F. Tian, Z. Song, and T. A. Cross, Orientational constraints derived from hydrated powder samples by two-dimensional PISEMA, *J. Magn. Reson.* **135,** 227–231 (1998).

34. A. Ramamoorthy and S. J. Opella, Two-dimensional chemical shift/heteronuclear dipolar coupling spectra obtained with polarization inversion spin exchange at the magic angle and magic angle sample spinning (PISEMAMAS), *Solid-State NMR* **4,** 387–392 (1995).

35. A. Ramamoorthy, L. M. Gierasch, and S. J. Opella, Resolved two-dimensional anisotropic chemical shift/heteronuclear dipolar coupling powder pattern spectra by three-dimensional solid-state NMR spectroscopy, *J. Magn. Reson. B* **110,** 102–106 (1996).

36. C. H. Wu, A. Ramamoorthy, L. M. Gierasch, and S. J. Opella, Simultaneous characterization of the amide ^{1}H chemical shift, ^{1}H–^{15}N dipolar, and ^{15}N chemical shift interaction tensors in a peptide bond by three-dimensional solid-state NMR spectroscopy, *J. Am. Chem. Soc.* **117,** 6148–6149 (1995).

37. A. Ramamoorthy, C. H. Wu, and S. J. Opella, Magnitudes and orientations of the principal elements of the ^{1}H chemical shift, ^{1}H–^{15}N dipolar coupling, and ^{15}N chemical shift interaction tensors in $^{15}N_{\varepsilon 1}$-tryptophan and $^{15}N_{\varepsilon}$-histidine side chains determined by three-dimensional solid-state NMR spectroscopy of polycrystalline samples, *J. Am. Chem. Soc.* **119,** 10479–10486 (1997).

38. G. A. Lorigan, R. McNamara, R. A. Jones, and S. J. Opella, Magnitudes and orientations of the ^{15}N chemical shift and ^{1}H–^{15}N dipolar coupling tensors of [1-^{15}N]-2′-deoxyguanosine determined on a polycrystalline sample by two-dimensional solid-state NMR spectroscopy, *J. Magn. Reson.,* in press (1999).

39. M. Mehring and J. S. Waugh, Magic angle NMR experiments in Solids, *Phys. Rev. B* **5,** 3459 (1972).

40. A. Bielecki, A. C. Kolbert, and M. Levitt, Frequency-switched pulse sequences: Homonuclear decoupling and dilute spin NMR in solids, *Chem. Phys. Lett.* **155,** 341 (1989)

41. A. Bielecki, A. C. Kolbert, H. J. M. de Groot, R. G. Griffin, and M. H. Levitt, *Adv. Magn. Reson.* **14,** 111 (1990).

42. M. Ravikumar and A. Ramamoorthy, Exact evaluation of the line-narrowing effect of the Lee–Goldburg pulse solid-state NMR spectroscopy, *Chem. Phys. Lett.* **286,** 199–204 (1988).

43. B.-J. Van Rossum, H. Forster, and H. J. M. De Groot, High-field and high-speed CP-MAS ^{13}C NMR heteronuclear dipolar-correlation spectroscopy of solids with frequency-switched Lee–Goldburg homonuclear decoupling, *J. Magn. Reson.* **124,** 516–519 (1997).

44. D. P. Burum and A. Bielecki, WIMSE, a new spectral editing technique for CPMAS solid-state NMR, *J. Magn. Reson.* **95,** 184–190 (1991).

45. R. R. Ernst, G. Bodenhausen, and A. Wokaun, "Principles of Nuclear Magnetic Resonance in One and Two Dimensions," Clarendon Press, Oxford (1986).